IOPscience iopscience.iop.org

Home Search Collections Journals About Contact us My IOPscience

Electron holography on silicon microstructures and its comparison to other microscopic techniques

This article has been downloaded from IOPscience. Please scroll down to see the full text article.

2004 J. Phys.: Condens. Matter 16 S193

(http://iopscience.iop.org/0953-8984/16/2/022)

View the table of contents for this issue, or go to the journal homepage for more

Download details:
IP Address: 129.252.86.83
The article was downloaded on 28/05/2010 at 07:16

Please note that terms and conditions apply.

INSTITUTE OF PHYSICS PUBLISHING JOURNAL OF PHYSICS: CONDENSED MATTER

J. Phys.: Condens. Matter **16** (2004) S193–S200 PII: S0953-8984(04)66992-X

Electron holography on silicon microstructures and its comparison to other microscopic techniques

Petr Formánek[1] **and Martin Kittler**

IHP GmbH—Innovations for High Performance Microelectronics,
Institut für Innovative Mikroelektronik, Im Technologiepark 25, D-15236 Frankfurt (Oder), Germany

E-mail: formanek@ihp-microelectronics.com

Received 31 July 2003
Published 22 December 2003
Online at stacks.iop.org/JPhysCM/16/S193 (DOI: 10.1088/0953-8984/16/2/022)

Abstract

Two-dimensional dopant profiling is being strongly demanded by the semiconductor industry, and several techniques have been developed in recent years. We compare the performance of electron holography in a transmission electron microscope with other microscopic techniques. The advantages of electron holography are the high spatial resolution of a few nanometres and the direct interpretability of the measured two-dimensional electrostatic potential requiring no simulation. We demonstrate the detection of a 0.5 monolayer of boron in silicon and silicon germanium. We image a 35 nm wide potential dip of 25 mV in a boron-doped specimen, corresponding to detection of a 2×10^{17} B cm^{-3} dip between peaks of 2×10^{18} B cm^{-3}. Moreover, we illustrate directly by electron holography the existence of a potential barrier at $NiSi_2$ precipitates in silicon, which was predicted earlier by the electron-beam-induced current technique.

1. Introduction

Scanning probe techniques and other microscopic methods are widely used in the area of semiconductors for characterization of semiconductor materials, crystal defects and device structures. Because the precise placement of dopants is critical for the device performance, techniques for two-dimensional dopant profiling are being strongly demanded by the semiconductor industry. The 2001 ITRS Roadmap [1] requires resolution of 2 nm and precision of 4% in the measurements of the dopant concentration by the year 2003. Several scanning probe techniques aiming at 2D dopant profiling have emerged over the last few years.

Scanning spreading resistance microscopy (SSRM) measures the local resistance of the specimen using a hard conductive tip with a small radius [2]. The achievable resolution,

[1] Author to whom any correspondence should be addressed.

10–20 nm, is determined by the contact radius given by the tip sharpness [3]. A recent report is given in [4]. A strong force has to be applied to make good contact between the specimen and the tip, which leads to scratching of the specimen and rapid wear of the tip. The advantage is that the method is quantifiable and has a high dynamic range of 10^{15}–10^{20} cm^{-3}.

Scanning capacitance microscopy (SCM) measures the local capacitance or the capacitance–voltage dependence of the specimen covered with a thin oxide layer [5]. Similarly to the SSRM, the resolution reaching 10–20 nm depends on the tip radius and the interaction volume with the specimen [3]. The technique is difficult to quantify since extensive simulation of tip–specimen interaction is necessary. Moreover, a bias applied to the tip causes movement in the junction. There are also problems with non-monotonic response to doping [6]. SCM is useful for the analysis of low-doped specimens since the sensitivity decreases as the specimen doping approaches the doping of the measuring tip.

The technique of electron-beam-induced current (EBIC) has also been used for delineation of the p–n junction and for channel length measurement in field effect transistors, e.g. [7], and even gives information on dopant profiles, e.g. [8]. Perovic *et al* [9] reported on dopant contrast by using secondary electrons (SE) in a field emission SEM. The contrasts were interpreted in terms of band bending effects between n- and p-doped layers. In [10] it was demonstrated that this contrast effect could be used for obtaining 2D dopant profiles from the SE images provided that the technique is empirically calibrated. Differently doped p-type regions can be usually imaged but n-doped regions show extremely low contrast and energy filtering of SE has to be used [11].

Electron holography is also a promising candidate for dopant profiling [12–15]. The off-axis electron holography is based on the interference of a reference electron wave having passed through vacuum and an object electron wave having passed through the specimen. The interferogram is recorded with a CCD camera and evaluated by image processing techniques [16]. The local phase shift of the electron wave is proportional to the local electrostatic potential distribution across the p–n junction [14]. The phase image can therefore be directly interpreted as a map of electrostatic potential, whereas the amplitude image corresponds to the conventional bright field image (see below, e.g. figure 3).

Unfortunately, the performance of the above techniques does not meet the requirements of the roadmap. Although even electron holography cannot fulfill the requirements completely, it exhibits a better performance in some aspects (atomic resolution possible in principle, relative ease of interpretation) as compared to the techniques described above. We demonstrate here the detection of a boron sub-monolayer in Si and SiGe and the detection of potential gradient of above 1 mV nm^{-1}, spreading over an area of 40 nm $\times$ 100 nm. An example for application of electron holography to P-MOS and N-MOS field effect transistors is also given. Moreover, electron holography allows a direct visualization of space charges/depletion layers around crystal defects. This will be shown here for small $NiSi_2$ precipitates in Si.

2. Demonstration of spatial resolution

As noted in the introduction, the achievable spatial resolution corresponds to the resolution of TEM. Only small areas (around 20 nm $\times$ 20 nm) can be imaged with atomic resolution. For larger objects, such as transistors, the resolution amounts to a few nanometres. In this section we show that sub-monolayer boron sheets in silicon and silicon germanium can be successfully imaged by using a Philips CM300/FEG microscope equipped with a Lorentz lens with a point resolution of 2 nm. Figure 1(b) shows the phase image of a structure schematically described in figure 1(a). The structure consists of MBE grown 90 nm thick layers of Si, $Si_{0.95}Ge_{0.05}$, $Si_{0.90}Ge_{0.10}$, $Si_{0.85}Ge_{0.15}$, and $Si_{0.80}Ge_{0.20}$ with a 0.5 monolayer of boron in the middle of each layer. The boron layers appear in the phase image as dark lines. The bright lines visible

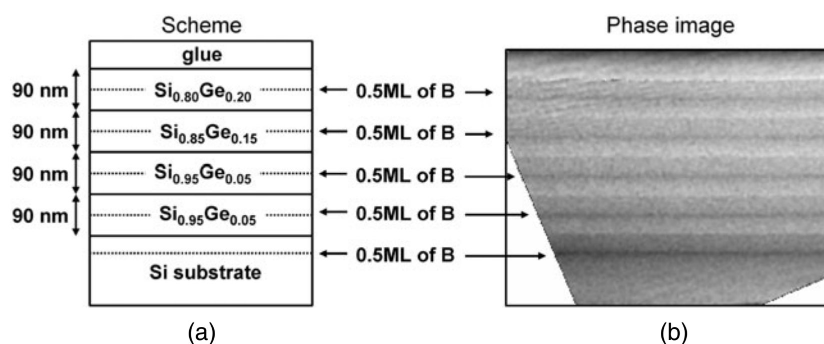

Figure 1. Scheme and phase image deduced from the electron hologram of a MBE grown structure used for the test of spatial resolution. 0.5 monolayers of boron in between a 90 nm thick Si layer and SiGe layers (5%, 10%, 15% and 20% of Ge) are visible as dark lines.

at the interface of the SiGe layers are artifacts caused by an undesired underfocusing. The highest spatial frequency contained in the image is $1/7\ \text{nm}^{-1}$. Electron holography images the doping indirectly through electrostatic potential redistribution caused by charge carriers. Therefore sub-monolayers of dopants are made visible due to their electrical activity spreading over several nanometres. The resolution achievable by electron holography is thus limited not by electron optics but by the Debye length.

3. Demonstration of detection limit and comparison to SIMS

Another important parameter is the detection limit which is related to the noise. The usual noise level in the phase image corresponds to a potential of about 100 mV. However, in the case of one-dimensional structures it could be reduced by about ten times by averaging. The structure investigated here consists of several layers with different boron concentration. The SIMS profile is displayed in figure 2(a), and the phase image is shown in figure 2(b). There are nine peaks labelled ‘A’ to ‘J’ in the structure. The peaks ‘H’ and ‘J’ are below the detection limit of holography. Peaks ‘F’ and ‘G’ are rather faint, whereas peaks ‘A’ to ‘E’ are clearly visible. A single linescan does not reveal the peaks ‘F’ and ‘G’. Averaging over at least 30 pixels (corresponding to linescan width of 100 nm) is necessary to filter them out of the noise. The valley between peaks ‘G’ and ‘F’ is 25 mV ‘deeper’ than the peaks and the distance between the peaks is about 80 nm. From these observations we conclude that a potential change of about 25 mV spreading over 40 nm in a one-dimensional structure can be detected after averaging over 100 nm. The ability to resolve peaks ‘G’ and ‘F’ corresponds to a detection limit of a 2×10^{17} B cm^{-3} dip between $\sim 2 \times 10^{18}$ B cm^{-3} peaks, which is—according to our knowledge—the best sensitivity that could be achieved by holography so far for Si-based structures.

Figure 2(a) shows a comparison of the potential calculated from the SIMS data with the potential measured by holography (linescan averaged over 300 nm). The measured potential corresponds very well with the calculated potential except for peak ‘A’. For such a high concentration of boron (4×10^{20} cm^{-3}) the amount of electrically active boron is smaller than the total concentration measured by SIMS. Indeed, conventional electron microscopy reveals nanoscopic particles, probably of boron silicide, in the position of layer ‘A’ (not shown here). Determination of the portion of active boron from the hologram is hardly possible due to the mixing of an ‘electrical’ signal from doped silicon and a ‘chemical’ signal from boron silicide particles.

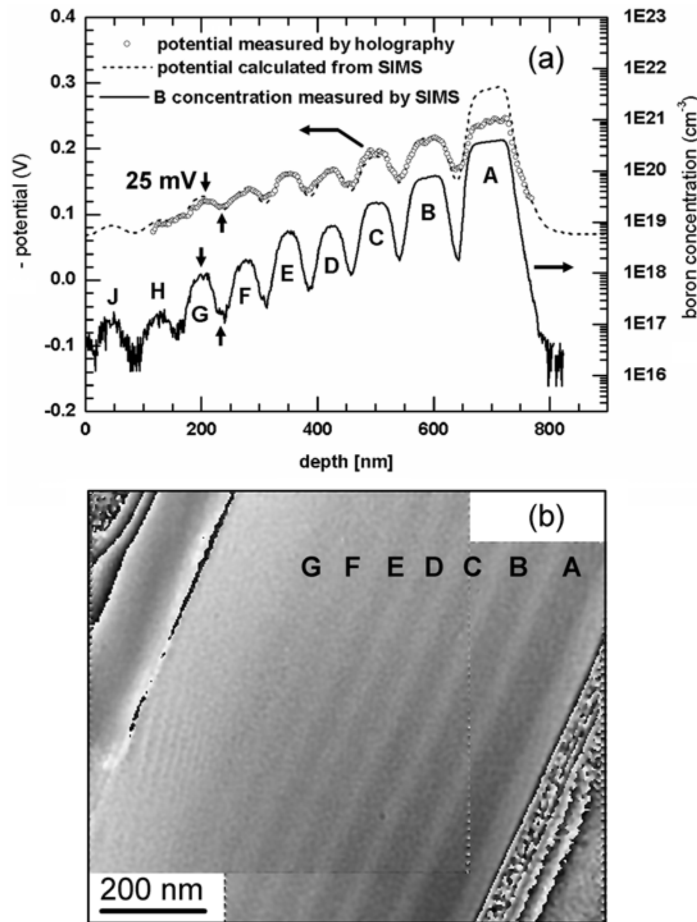

Figure 2. (a) Boron concentration profile and potential profile of a CVD grown structure used for testing the detection limit. See text for details about the calculated potential. (b) Phase image of the structure. A very high sensitivity of 25 mV could be achieved allowing the visualization of $\sim 10^{18}$ cm^{-3} boron peaks 'G' and 'F' separated by a 10^{17} cm^{-3} boron valley. Only the peaks 'H' and 'J' are below the detection limit.

4. Application to MOS transistors

Figure 3 shows a comparison of conventional bright field images with holograms taken from cross-sections of P-MOS (figures 3(a)–(c)) and N-MOS (figures 3(d)–(f)) transistors fabricated with quarter micrometre technology. The conventional bright field images (figures 3(a), (d)) and amplitude images (figures 3(b), (e)) show no contrast of the source/drain regions. The phase images (figures 3(c), (f)) reveal clearly the p-doped (dark areas) and the n-doped (bright areas) source/drain regions in P-MOS and N-MOS, respectively. The distribution of the electrostatic potential—which can be straightforwardly deduced from the experimentally determined phase image [14]—is related to the distribution of the dopant atoms. The specimen thickness was measured from the amplitude image by the method published in [22] using the inelastic mean-free path of 125 nm [23]. The potential drops across the p–n junctions in figure 3 were measured

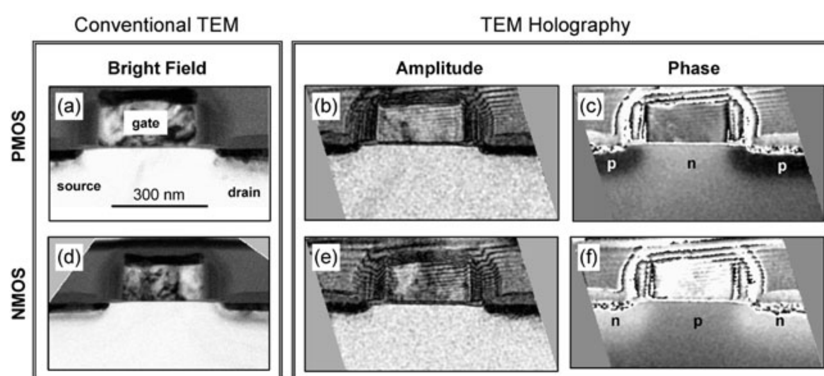

Figure 3. Cross-section images of P-MOS (a)–(c) and N-MOS (d)–(f) transistors. Conventional TEM bright field images (a), (d) and micrographs deduced from electron holograms: amplitude images (b), (e), and phase images (c), (f). The amplitude images contain basically the same information as bright field images. The phase images clearly reveal p- and n-doping in the source/drain areas.

to be 0.81 V for P-MOS and 0.64 V for N-MOS. These values are smaller than expected. One would expect 0.9 V from the design rules of the transistor. The difference might be accounted for by incorrect dead layer thickness (taken to be 25 nm [14] throughout this paper) or more probably for a potential reduction due to electron illumination. This will shortly be discussed below in the section on nickel silicide. The reason why the N-MOS does not have the same potential drop as the P-MOS cannot be understood at present.

An advanced specimen preparation technique was developed [17] and applied successfully for the preparation of more than 20 MOS, bipolar and heterobipolar transistors during the last year.

5. Study of $NiSi_2$ precipitates in silicon

$NiSi_2$ precipitates in Si can be formed under suitable conditions without the occurrence of any secondary defects, e.g. [18]. This allows one to use them as 'model defects' for studying the electrical activity of metal silicide precipitates in Si. We could show with EBIC that small $NiSi_2$ precipitates (diameter less than 1 μm, thickness about 10–20 nm) are efficient recombination centres leading to surprisingly strong activity. For n-type Si doped with 4×10^{14} P cm^{-3} a maximum contrast of about 0.4 was measured at room temperature [19]. Moreover, it was shown that the minority carrier diffusion length L_D is related to the precipitate density N_{EBIC} via $L_D \sim 0.7 \times N_{EBIC}^{-1/3}$. Hence, $NiSi_2$ precipitates form a dominant recombination path for charge carriers.

As a possible reason for this large recombination activity, space charge regions (SCRs) around the particles were proposed which could strongly increase the effective capture cross-section for minority carriers. In other words, the strong activity of the precipitates is explained as a consequence of Schottky barriers forming a potential barrier/band bending around the particles. Recently, this hypothesis could be encouraged by a quantitative model [20]. From investigations of the dependence of the EBIC contrast on temperature and beam current $c(T, I_b)$ the potential barrier Φ was deduced [21]. Φ was found to depend on dopant concentration, temperature and injection level. It decreased with growing injection level (beam current) and the barrier in the dark was estimated to be about $\Phi_{dark} \sim 0.4$–0.5 V at 300 K for a doping of 4×10^{14} P cm^{-3}.

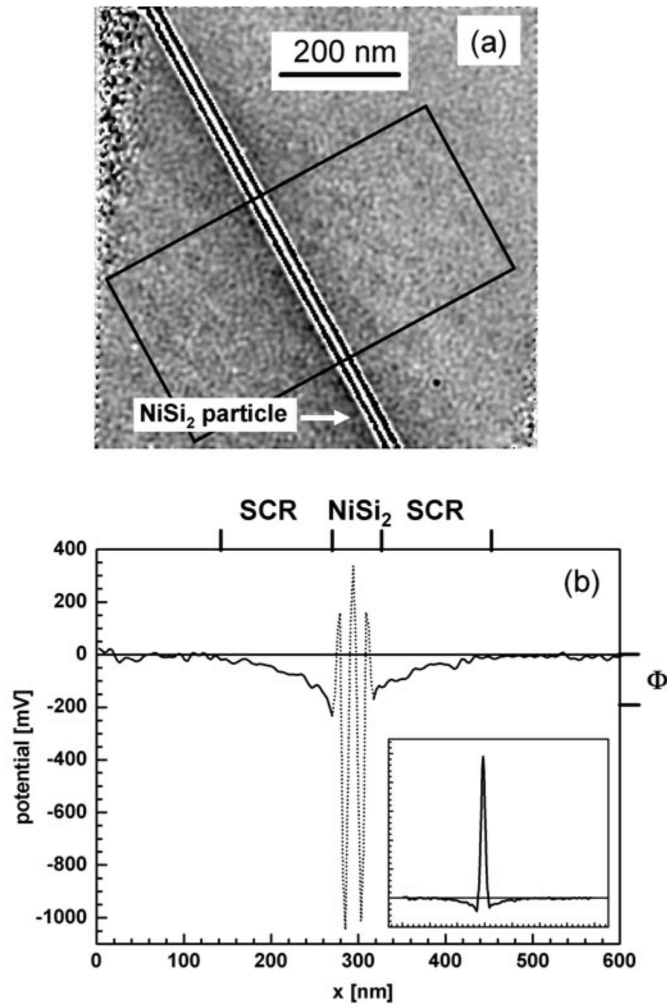

Figure 4. (a) Phase image of a $NiSi_2$ precipitate in n-type Si viewed nearly edge-on. The rectangle marks the area used for an averaged linescan. (b) Potential profile in a direction perpendicular to the precipitate as indicated in the phase image. The potential barrier $\Phi = U_{holo} \sim 0.15$–0.20 V and SCR are marked. The dotted part of the curve corresponds to the mean inner potential in $NiSi_2$. The jumps are due to the phase wrapping (i.e. phase shift φ larger than 2π is represented as φ modulo 2π). The inset shows the unwrapped phase schematically.

Consequently, from quantitative EBIC investigations, Schottky barrier effects were proposed as the origin of the electrical activity of $NiSi_2$ precipitates. However, according to our knowledge a direct verification of this view has been missing up to now. Electron holography seems to be a suitable tool for such a verification. Indeed, we observed a potential decrease in the vicinity of $NiSi_2$ precipitates in an n-doped substrate, indicating the existence of a potential barrier. Figure 4(a) shows a phase image of a precipitate viewed approximately along the $\langle 110 \rangle$ direction. The specimen was tilted by about 10° off the zone axis to minimize dynamical diffraction effects, but with the $NiSi_2$/Si interface kept nearly edge-on. The dark surrounding the precipitate corresponds to the lower potential. The linescan from the phase image averaged over 100 pixels and calibrated to potential is plotted in figure 4(b). The

Table 1. Comparison of two-dimensional dopant profiling techniques.

Method	Resolution (nm)	Measurement area	Quantifiable	Dynamic range
Electron holography	5–10[a]	500 nm–1.3 μm	Yes	High doping ($>10^{18}$ cm^{-3})
EBIC	10[b]	1 μm to tens of μm	Limited	
SE contrast	5–10	1 μm to tens of μm	Very difficult (empirical calibration)	$>10^{16}$ cm^{-3}
SCM	10–20	1 μm to tens of μm	Extremely difficult (empirical calibration)	Low doping
SSRM	10–20	1 μm to tens of μm	Yes	10^{15}–10^{20} cm^{-3}

[a] Atomic resolution is possible in principle for potential mapping. Resolution in doping is limited by the Debye length.
[b] Junction position.

dotted part of the curve corresponds to the mean inner potential in $NiSi_2$ (it is a chemically sensitive signal). The jumps are due to so called phase wrapping: phase shift φ larger than 2π is represented as φ modulo 2π. The inset shows the unwrapped phase schematically only, without scale.

The height of the potential barrier can be estimated to be $U_{\text{holo}} \sim 0.15$–0.20 V from the phase shift determined by holography and the specimen thickness. The thickness of the silicon substrate was measured by CBED and amounts to (420 ± 20) nm. The dimensions of the $NiSi_2$ precipitate are roughly 440 nm $\times$ 30 nm $\times$ 7 μm according to measurements from several projections of the particle. The height of the barrier deduced from holography $U_{\text{holo}} \sim 0.15$–0.20 V is lower than the value $\Phi_{\text{dark}} \sim 0.4$–0.5 V.

The specimen is excited by 300 keV electrons with a current density of the order of 10^{-2}–10^{-3} A cm^{-2}. The excess electron–hole pairs being generated this way reduce the band bending of the Schottky barrier which exists around the precipitate. They cause an open circuit voltage, acting as a forward bias on the barrier. This voltage drop can be estimated from the difference $\Delta U = \Phi_{\text{dark}} - U_{\text{holo}}$ to yield about 0.3 V. This rather high value is found for low substrate doping (4×10^{-14} cm^{-3}). It corresponds quite well to the value estimated from the relation [24] $\Delta U = kT/e \ln(1 + J_G/J_S)$, where kT/e is the thermal voltage, J_G is the generation current (10^{-3} A cm^{-2}) and J_S denotes the reverse current (10^{-9} A cm^{-2}) of the Schottky barrier. For a highly doped p–n junction (5×10^{18} cm^{-3}) we observed a voltage drop of $\Delta U \sim 0.18$ V [23], which is smaller than the value found here. This is in agreement with our observation discussed in section 3.

Hence, due to the generation of excess carriers by the incident electrons the potential deduced from holography is smaller than the built-in potential. Consequently, a simple straightforward interpretation of the phase may lead to errors in the absolute measurements of potential.

6. Conclusions

Although there is no technique that can fulfill the requirements of the ITRS Roadmap, SCM, SSRM and electron holography are fast approaching them. Exact quantitative comparison of the methods is not possible since the techniques use different principles and different approaches to the issues like resolution and sensitivity. We summarize the comparison in table 1.

Using electron holography we detected a 0.5 monolayer of boron in silicon and silicon germanium. We imaged a 35 nm wide potential dip of 25 mV in a boron-doped specimen,

corresponding to detection of a 2×10^{17} B cm^{-3} dip between $\sim 2 \times 10^{18}$ B cm^{-3} peaks. There are still several problems in electron holography such as specimen charging and excess carrier generation under electron illumination which affects the built-in potential, the 'dead layer' at the specimen surfaces, and the dynamical diffraction contribution to the measured phase (mechanical stress in the specimen, bending of the specimen, disturbance due to crystal defects).

Schottky barriers at $NiSi_2$ precipitates in silicon as predicted by EBIC could be confirmed by electron holography allowing a direct imaging of the potential barrier.

Acknowledgments

We would like to acknowledge M Seibt for providing the $NiSi_2$ specimen, H Rücker for the specimen with transistors, Y Yamamoto for the specimen with boron layers, W-D Rau for the specimen with boron deltas in SiGe, and R Kurps for the SIMS measurement. We are grateful to P Schwander for fruitful discussions. P Formánek acknowledges the EU-Project HERCULAS for funding of his studentship.

References

[1] International Technology Roadmap for Semiconductors 2001, section Metrology http://public.itrs.net/Files/2001ITRS/Home.htm
[2] De Wolf P, Clarysse T, Vandervorst W, Snauwaert J and Hellemans L 1996 *J. Vac. Sci. Technol.* B **14** 380
[3] De Wolf P, Stephenson R, Trenkler T, Clarysse T, Hantschel T and Vandervorst W 2000 *J. Vac. Sci. Technol.* B **18** 361
[4] Alvarez D, Hartwich J, Fouchier M, Eyben P and Vandervorst W 2003 *Appl. Phys. Lett.* **82** 1724
[5] McMurray J S, Kim J and Williams C C 1997 *J. Vac. Sci. Technol.* B **15** 1011
[6] Duhayon N, Clarysse T, Eyben P, Vandervorst W and Hellemans L 2002 *J. Vac. Sci. Technol.* B **20** 741
[7] Kittler M and Lärz J 1998 *Solid State Phenom.* **63/64** 77
[8] Rechenberg I, Wenzel H, Knauer A and Beister G 1998 *Solid State Phenom.* **63/64** 69
[9] Perovic D D, Castell M R, Howie A, Lavoie C, Tiedje T and Cole J S W 1995 *Ultramicroscopy* **58** 401
[10] Venables D and Maher D M 1996 *J. Vac. Sci. Technol.* B **14** 421
[11] Schönjahn C, Humphreys C J and Glick M 2002 *J. Appl. Phys.* **92** 7667
[12] Frabboni S, Matteucci G, Pozzi G and Vanzi M 1985 *Phys. Rev. Lett.* **55** 2196
[13] McCartney M R, Smith D J, Hull R, Bean J C, Völkl E and Frost B 1994 *Appl. Phys. Lett.* **65** 2603
[14] Rau W D, Schwander P, Baumann F H, Höppner W and Ourmazd A 1999 *Phys. Rev. Lett.* **82** 2614
[15] Gribelyuk M A, McCartney M R, Li J, Murthy C S, Ronsheim P, Doris B, McMurray J S, Hegde S and Smith D J 2002 *Phys. Rev. Lett.* **89** 25502
[16] Völkl E, Allard L F and Joy D C (ed) 1999 *Introduction to Electron Holography* (New York: Kluwer–Academic) ISBN 030644920X
[17] Formanek P and Bugiel E 2003 *Ultramicroscopy* submitted
[18] Seibt M and Schröter W 1989 *Phil. Mag.* A **59** 337
[19] Kittler M, Lärz J, Seifert W, Seibt M and Schröter W 1991 *Appl. Phys. Lett.* **58** 911
[20] Plekhanov P S and Tan T Y 2000 *Appl. Phys. Lett.* **76** 3777
[21] Kittler M and Seifert W 1995 *Phys. Status Solidi* a **150** 463
[22] McCartney M R and Gajdardziska-Josifovska M 1994 *Ultramicroscopy* **53** 283
[23] Formanek P 2003 *PhD Thesis* in preparation
[24] Sze S M 1981 *Physics of Semiconductor Devices* (New York: Wiley)